Nigerian Journal of Physics (NJP)
ISSN online: 3027-0936
ISSN print: 1595-0611
DOI: https://doi.org/10.62292/njp.v34i2.2025.359
Volume 34(2), June 2025

Tailoring Structural, Morphological, and Photocatalytic Properties of ZnO-ZrO2 Nanocomposites: Influence of Calcination Temperature

[1]Midala, I. H., *[1,2]Wante, H. P. and [1]Nuhu, I. M.

[1]Department of Science Laboratory Technology, Federal Polytechnic Mubi, Adamawa State, Nigeria.
[2]Plasma Technology Research Centre, Department of Physics, Faculty of Science, University Malaya, Kuala Lumpur, Malaysia, 50603.

*Corresponding author's email: wante2h@gmail.com

ABSTRACT

This study presents the synthesis and characterization of (ZnO)0.8(ZrO2)0.2 nanocomposites using a polyvinylpyrrolidone (PVP)-assisted thermal route, with calcination temperatures ranging from 500 °C to 800 °C. X-ray diffraction (XRD) confirmed the coexistence of hexagonal ZnO and monoclinic ZrO_2 phases, with crystallinity progressively improving with temperature. Crystallite sizes increased from ~11.0 nm at 500 °C to ~32.5 nm at 800 °C, as confirmed by both XRD and high-resolution transmission electron microscopy (TEM). Morphological evolution demonstrated controlled particle growth and uniform dispersion, while photoluminescence (PL) spectra revealed enhanced near-band-edge emissions and reduced deep-level emissions at higher temperatures, indicating suppressed electron–hole recombination. Notably, calcination at 700–800 °C provided an optimal balance between crystallinity and defect passivation. These results highlight the critical role of calcination temperature in tailoring structural, morphological, and optical properties, thereby enhancing the photocatalytic efficiency of ZnO-ZrO2 composites for potential use in energy conversion and environmental remediation technologies.

Keywords: Semiconductor, Nanocomposite, Calcination, Crystallinity, $(ZnO)_{0.8}$ $(ZrO_2)_{0.2}$.

INTRODUCTION

Semiconductor nanoparticles have attracted significant interest due to their tunable optical, electrical, and chemical properties, making them indispensable in a wide range of applications, including biomedicine, luminescence, photocatalysis, solar cells, display panels, and single-electron transistors (Liao *et al.*, 2006; Terna *et al.*, 2021). Among these materials, zirconium dioxide (ZrO_2) has emerged as a promising n-type semiconductor, characterized by its wide band gap energy (5.0–5.5 eV) Sathyaseelan *et al.* (2017), high thermal stability, excellent chemical resistance, and ability to function as a photocatalyst. However, its large band gap restricts its photocatalytic efficiency under visible light, necessitating strategies such as doping with transition metal ions or forming composites with other metal oxides to enhance its optoelectronic properties (Park *et al.*, 2017).

Zinc oxide (ZnO) has been widely investigated as an n-type semiconductor due to its low cost, facile synthesis, high optical absorption, and superior photocatalytic properties (Lee *et al.*, 2016; Sun *et al.*, 2023). ZnO exhibits a band gap of approximately 3.37 eV and an exciton binding energy of around 60 meV, making it an excellent candidate for photocatalysis, ultraviolet (UV) detection, and optoelectronic applications (López *et al.*, 2019; Yousefi *et al.*, 2018). Compared to titanium dioxide (TiO_2), another extensively used photocatalyst, ZnO offers a broader absorption range in the solar spectrum, further increasing its potential for light-driven catalytic processes (Yousefi *et al.*, 2018). The combination of ZnO with ZrO_2 has been shown to enhance photocatalytic performance due to synergistic effects, including improved charge separation efficiency, higher density of states, and better stability under irradiation (Kamari *et al.*, 2019; Zhang *et al.*, 2017).

The synthesis of ZnO-ZrO_2 nanocomposites through combustion-based processes offers an efficient route for producing high-purity materials with controlled particle size and minimal byproducts, thereby ensuring environmental sustainability (Al-Hada *et al.*, 2016). This approach aligns with green chemistry principles, as highlighted by Kamari *et al.* (2019), emphasizing energy efficiency, cost-effectiveness, and product quality. The

resulting nanomaterials, featuring hexagonal ZnO and tetragonal ZrO_2 crystalline phases, belong to the group II-VI composite materials and exhibit unique optoelectronic characteristics due to their nanoscale dimensions (Vitor *et al.*, 2015). The ability of these nanocomposites to modify their band structure by tuning the ZnO:ZrO_2 ratio provides a versatile platform for optimizing performance in specific applications, including pollutant degradation, antibacterial agents, and advanced electronic devices (Mariyappillai *et al.*, 2025; Precious Ayanwale & Reyes-López, 2019).

Previous studies Deepika and Veerakumar (2024); López *et al.* (2019); Shakir *et al.* (2024), have demonstrated the effectiveness of ZnO-ZrO_2 composites in photocatalytic applications. Notably, Zn_2Zr, a photocatalyst comprising ZnO and ZrO_2 in a 2:1 molar ratio, has shown remarkable efficiency in degrading organic pollutants, benefiting from the reduced band gap and enhanced charge carrier separation (Sherly *et al.*, 2014). Similarly, nanocomposites with a ZrO_2:ZnO ratio of 1:2 have been reported to exhibit superior photocatalytic activity due to an optimized electronic structure and improved stability under light exposure (Gurushantha *et al.*, 2017). These enhanced properties stem from the synergistic interactions between ZnO and ZrO_2, leading to improved light absorption, efficient electron transport Kubiak *et al.* (2018), and reduced recombination rates of electron-hole pairs, thereby enhancing their functional performance in environmental and energy-related applications.

Building on our prior work Midala *et al.* (2019), which focused on the synthesis of binary oxide $(ZnO)_{0.2}(ZrO_2)_{0.8}$ nanoparticles through heat treatment at different temperatures, the present study explores the fabrication of a novel ZnO-ZrO_2 nanocomposite with varying proportions, specifically $(ZnO)_{0.8}(ZrO_2)_{0.2}$, using a controlled calcination process. This new composition integrates both organic and inorganic nanoparticles, aiming to enhance photocatalytic efficiency. A key objective of this study is to synthesize and analyze a nanocomposite powder doped with $(ZnO)_x(ZrO_2)_{1-x}$ via thermal treatment, with the goal of developing an advanced material that surpasses existing ZnO-ZrO_2 composites in terms of photocatalytic performance. The structural, optical, and electronic properties of the synthesized nanocomposites was systematically investigated to elucidate the underlying mechanisms governing their enhanced activity and stability under irradiation.

Furthermore, the present study aims to understand the role of different synthesis parameters, including temperature variations, doping concentrations, and calcination durations, in tailoring the physicochemical properties of ZnO-ZrO_2 composites. The structural, morphological, and optical properties of these nanocomposites will be analyzed using advanced characterization techniques such as X-ray diffraction (XRD), transmission electron microscopy (TEM), and photoluminescence (PL) spectroscopy. These insights will not only contribute to optimizing synthesis techniques but also pave the way for expanding the applicability of ZnO-ZrO_2 composites in energy conversion, environmental remediation, and optoelectronic devices.

By leveraging the advantages of ZnO-ZrO_2 nanocomposites, this research seeks to push the boundaries of semiconductor materials engineering, providing innovative solutions for sustainable and high-performance photocatalytic materials. The findings of this study will have significant implications for the advancement of nanotechnology-driven solutions in environmental sustainability and energy-efficient applications.

MATERIALS AND METHODS

Materials

Zn $(NO_3)_2.6H_2O$ (MW=297.37 g/mol) and Zr $(NO_3)_4.5H_2O$ (MW= 439.32 g/mol), polyvinylpyrrolidone (PVP MW=55,000 g/mol) were purchase from Sigma Aldrich. Other materials are di-onized water, magnetic stirrer and petri dish.

Method

PVP weighing 4 g was dissolved in 100 ml of deionized water under the influence of a magnetic stirrer. Subsequently, 0.2 moles of zinc nitrate hexahydrate (Zn $(NO_3)_2.6H_2O$) and 0.8 moles of zirconium (II) nitrate pentahydrate (Zr $(NO_3)_4.5H_2O$) were introduced and blended, ensuring the creation of a homogeneous solution through 1hour of continuous stirring at a temperature of 70°C.

The resulting solution, was subjected to a dehydration process lasting 24 hours at a controlled temperature of 80°C. The outcome of this meticulous procedure yielded a dry, white gel, which was subsequently pulverized into a finely textured powder. Figure 1 provide the flow of the synthesis method.

A portion of this powder was reserved for ambient temperature X-ray diffraction (XRD) analysis. The remaining powder was subdivided into four distinct samples, each of which underwent calcination at varying temperatures-500°C, 600°C, 700°C, and 800°C, each for a duration of 4 hours. This progressive thermal treatment aimed to explore the evolving characteristics of the binary oxides under different calcination conditions. The synthetic and calcined binary oxides thus obtained were meticulously prepared for subsequent in-depth characterization studies.

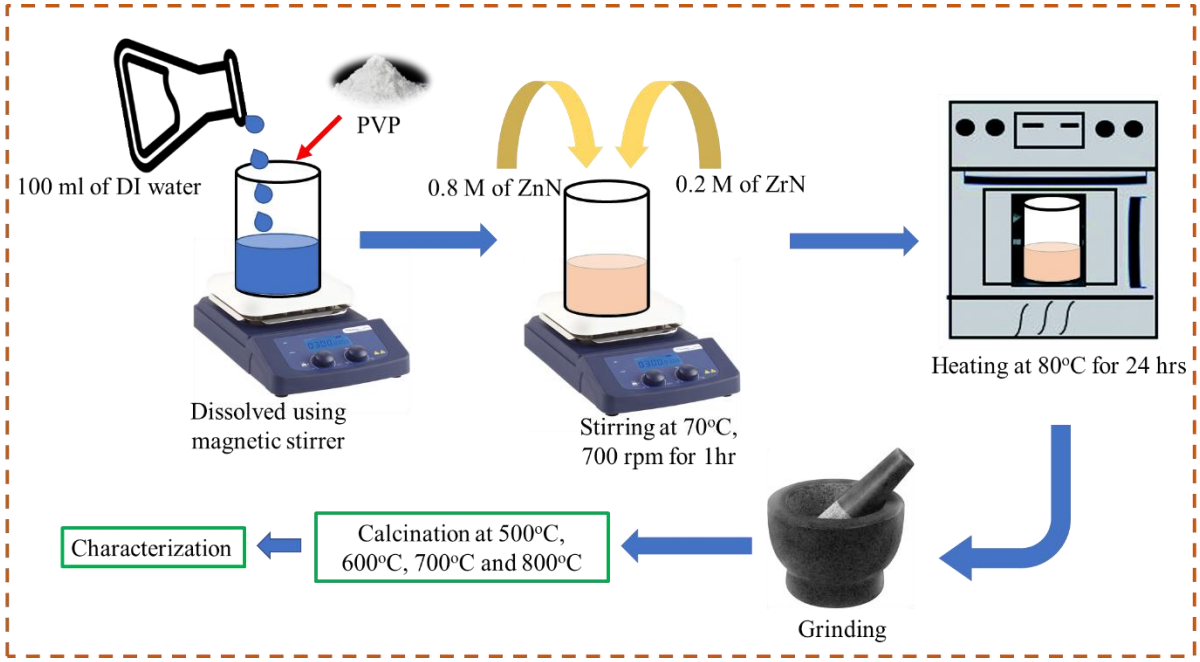

Figure 1: Schematic flow of the synthesis method

Characterization

XRD patterns for the specimens were acquired employing an EMPY-REAN diffractometer, utilizing Cu-Kα radiation, with a scan rate of 5/min, operating under conditions of 5 kV and 30 mA. The determination of crystalline values was executed through the application of Scherrer's formula, as defined in equation (1) (Wante *et al.*, 2021);

$$D = {}^{0.9\lambda}/_{\beta \cos \theta} \qquad (1)$$

where $\lambda =$ wavelength of $X-$ ray = 1.5406Å, β = Full width half maximum (FWHM) in radian and θ = angle of diffraction.

The crystalline sizes for $(ZnO)_{0.8}$ $(ZrO_2)_{0.2}$ were calculated using eq. 1. Transmission electron microscopy (TEM) (2010F UHR; JOEL) analysis was used to examined the characteristics of very tiny objects at an accelerating voltage of 200 kV. Photoluminescence (PL) (Parkin Elmer LS 55) analysis was performed on the calcinated samples in order to determine the photon emission of particles. The study was performed at room temperature on the calcined samples.

RESULTS AND DISCUSSION

Figure 2: illustrates the intricate interplay between PVP and metal ions in the heat treatment methodology employed for the synthesis of ZnO and ZrO nanocrystals. Robust ionic interactions between metallic ions and the amide groups within the polymeric chain effectively confine Zn and Zr ions (Gene *et al.*, 2015). PVP, employing steric and electrostatic stabilization mechanisms, serves to stabilize dissolved metallic salts. Preceding adsorption onto metallic ion surfaces, the PVP stabilizer may undergo partial breakdown, resulting in the formation of truncated polymer chains with capping (Koebel *et al.*, 2008). These shortened chains facilitate the uniform distribution of metallic ions within cavities and networks Midala *et al.* (2019), a phenomenon sustained until the cessation of the drying process.

Throughout these processes, Zr_4^+ and Zn_2^+ ions undergo oxidation during calcination, leading to the production of zinc oxide and zirconium oxide, respectively (Goodarz Naseri *et al.*, 2012).

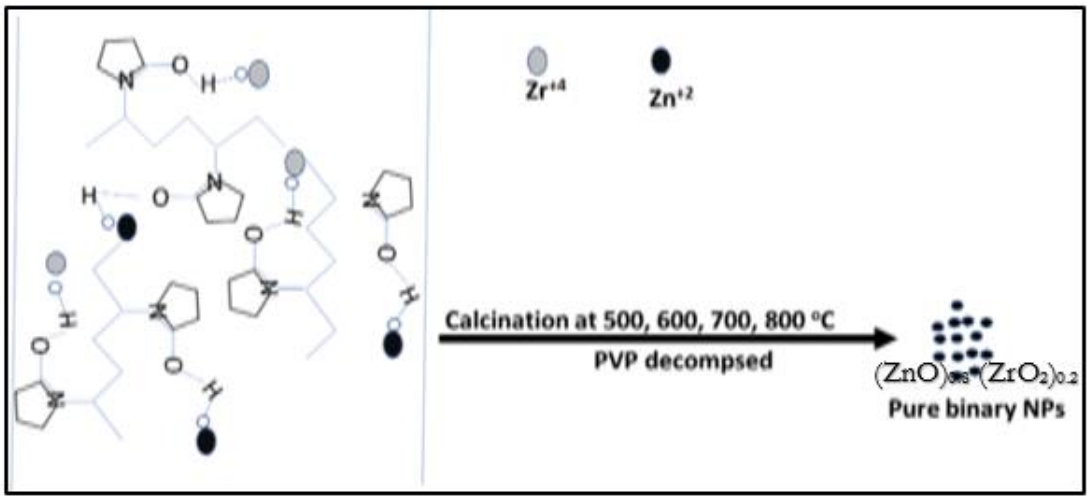

Figure 2: Interaction mechanism of metallic ions and PVP

Structural Analysis

Figure 3 shows the XRD patterns of the binary nanocomposite $(ZnO)_{0.8}(ZrO_2)_{0.2}$ prepared at room temperature (30°C) and subjected to calcination at 500°C, 600°C, 700°C, and 800°C which exhibit significant structural evolution, reflecting changes in crystallinity, phase composition, and peak intensities. The diffraction peaks match the standard JCPDS file No. 36-1451, confirming the presence of both ZnO (denoted by *) and ZrO_2 (denoted by #) phases in the composite material.

At room temperature (30°C), the XRD pattern shows weak and broad peaks, suggesting that the as-prepared sample is predominantly amorphous or nanocrystalline, with limited long-range order. The absence of sharp diffraction peaks at this stage implies that the material contains a high degree of structural disorder Cairns and Goodwin (2013), possibly due to incomplete crystallization during synthesis.

Upon calcination at 500°C, distinct ZnO diffraction peaks appear, corresponding to the characteristic wurtzite hexagonal structure of ZnO (Kayani *et al.*, 2015). The presence of peaks at 2θ values around 31.8° (*100), 34.4° (*002), 36.2° (*101), and 47.5° (*102) confirms the formation of crystalline ZnO. Additionally, weak diffraction peaks associated with the monoclinic phase of ZrO_2, such as #111 and #220, become evident. However, the broadening of peaks at this stage suggests that the crystallites remain relatively small, and some residual amorphous content may still be present.

At 600°C, the intensity of ZnO diffraction peaks increases, indicating an enhancement in crystallinity due to grain growth and the reduction of internal strain. The peaks associated with ZrO_2 also become more pronounced, suggesting improved phase separation between ZnO and ZrO_2. The narrowing of peak widths at this temperature implies an increase in crystallite size, as higher thermal energy facilitates atomic rearrangement and promotes grain coalescence (Kocjan *et al.*, 2017).

As the calcination temperature is further increased to 700°C, the XRD pattern shows sharper and more intense diffraction peaks, particularly for ZnO, confirming a well-developed crystalline structure. The increase in ZnO peak intensity suggests that grain growth is more pronounced, leading to a more ordered lattice with fewer defects. The diffraction peaks of ZrO_2 also become more distinct, indicating improved phase crystallization. The presence of both phases in the XRD spectrum confirms that ZrO_2 remains stable within the ZnO matrix without undergoing significant diffusion into the ZnO lattice.

At the highest calcination temperature of 800°C, the ZnO diffraction peaks exhibit maximum intensity, signifying the highest degree of crystallinity and the largest crystallite size achieved in the study. The enhanced peak sharpness suggests a reduction in microstrain and lattice imperfections (Vickers *et al.*, 2005). Additionally, the ZrO_2 peaks remain evident, indicating that the binary nanocomposite retains its phase integrity even at elevated temperatures. The increased thermal energy at 800°C likely facilitates the removal of residual defects and promotes optimal crystallization, leading to well-defined and thermally stable ZnO-ZrO_2 nanocomposites.

The XRD analysis reveals that increasing the calcination temperature enhances the crystallinity of ZnO and ZrO_2 phases while promoting grain growth and phase separation. Similar scenario was observed in the case of Al-Hada *et al.* (2014). The presence of distinct ZnO and ZrO_2 peaks at all temperatures confirms that the composite structure remains stable without significant interdiffusion. The improvement in structural order with increasing temperature suggests that calcination at 700°C or 800°C provides the optimal conditions for obtaining highly crystalline ZnO-ZrO_2 nanocomposites, which can be beneficial for applications requiring high structural stability and enhanced optical or electronic properties.

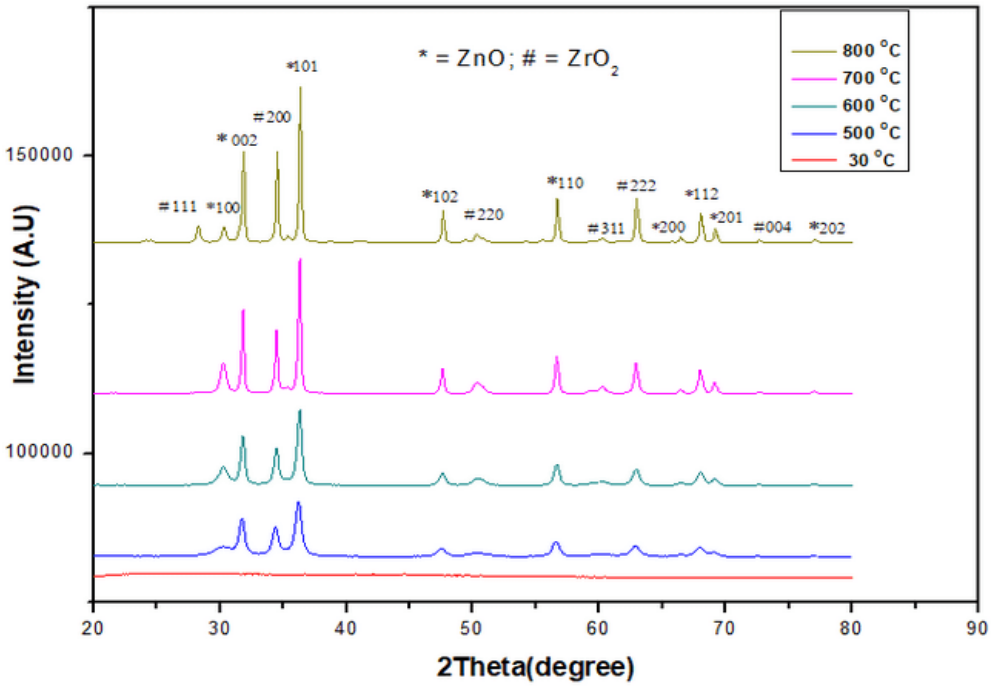

Figure 3: XRD models of binary nanocomposite $(ZnO)_{0.8}$ $(ZrO_2)_{0.2}$ prepared at (a) room temperature 30 ° C and calcination temperatures of (b) 500 (c) 600 (d)700 and (e) 800 ° C

Morphological analysis

Figure 4 presents high-resolution TEM images of $(ZnO)_{0.8}(ZrO_2)_{0.2}$ nanocomposites synthesized at different calcination temperatures (500°C, 600°C, 700°C, and 800°C). The corresponding particle size distributions provide insight into the impact of calcination temperature on nanoparticle growth and morphology. As the temperature increases, a noticeable trend in particle size evolution can be observed, confirming the role of thermal treatment in shaping nanocomposite structures.

At 500°C (Figure 4a), the nanocomposite exhibits a relatively small particle size, averaging 11 nm. The particles appear finely distributed, and the morphology remains uniform, indicating that at lower calcination temperatures, limited atomic diffusion restricts grain growth, thus maintaining a smaller crystallite size (Kamari *et al.*, 2017; Ullah *et al.*, 2010). The associated histogram confirms a narrow size distribution, suggesting minimal agglomeration at this stage.

With an increase in temperature to 600°C (Figure 4b), the average particle size grows to 17.5 nm, indicating enhanced atomic mobility and diffusion (Ullah *et al.*, 2010). The TEM image reveals a denser structure with slightly larger and more defined particles. The increase in size is likely attributed to grain boundary migration and coalescence effects, where adjacent particles begin to merge as the thermal energy overcomes surface energy barriers (Maaz *et al.*, 2009). Despite this growth, the morphology remains relatively uniform, suggesting controlled nucleation and crystal formation.

At 700°C (Figure 4c), the particle size further increases to 21 nm. The TEM image shows more distinct nanoparticles with well-defined edges, confirming improved crystallinity. At this stage, thermal energy promotes significant grain boundary mobility, leading to enhanced particle growth while still maintaining uniformity. The size distribution broadens slightly, suggesting that while most particles grow in a controlled manner, some begin to coalesce into larger grains.

A significant change is observed at 800°C (Figure 4d), where the particle size reaches 32.5 nm. The TEM image depicts larger, well-fused nanoparticles, indicating substantial grain growth due to increased diffusion and coarsening. This phenomenon occurs as smaller particles merge into larger ones, a typical behavior in high-temperature sintering processes. While this enhances crystallinity, excessive particle growth could lead to a reduction in the material's surface area, which may impact its performance in applications such as catalysis, adsorption, or sensing.

The results clearly demonstrate that calcination temperature plays a crucial role in determining nanoparticle size and morphology. The increasing trend in particle size, from 11 nm at 500°C to 32.5 nm at 800°C, highlights the effect of thermal energy in promoting atomic diffusion, grain growth, and crystallinity. However, excessive calcination at very high temperatures can lead to excessive grain growth,

potentially reducing the surface-to-volume ratio, which is critical for many applications.

These findings suggest that an optimal calcination temperature range (between 600°C and 700°C) may be ideal for maintaining a balance between particle size, crystallinity, and surface area. This balance is essential for tailoring nanocomposite properties for specific applications, ensuring that particle growth is controlled while preserving desirable structural characteristics.

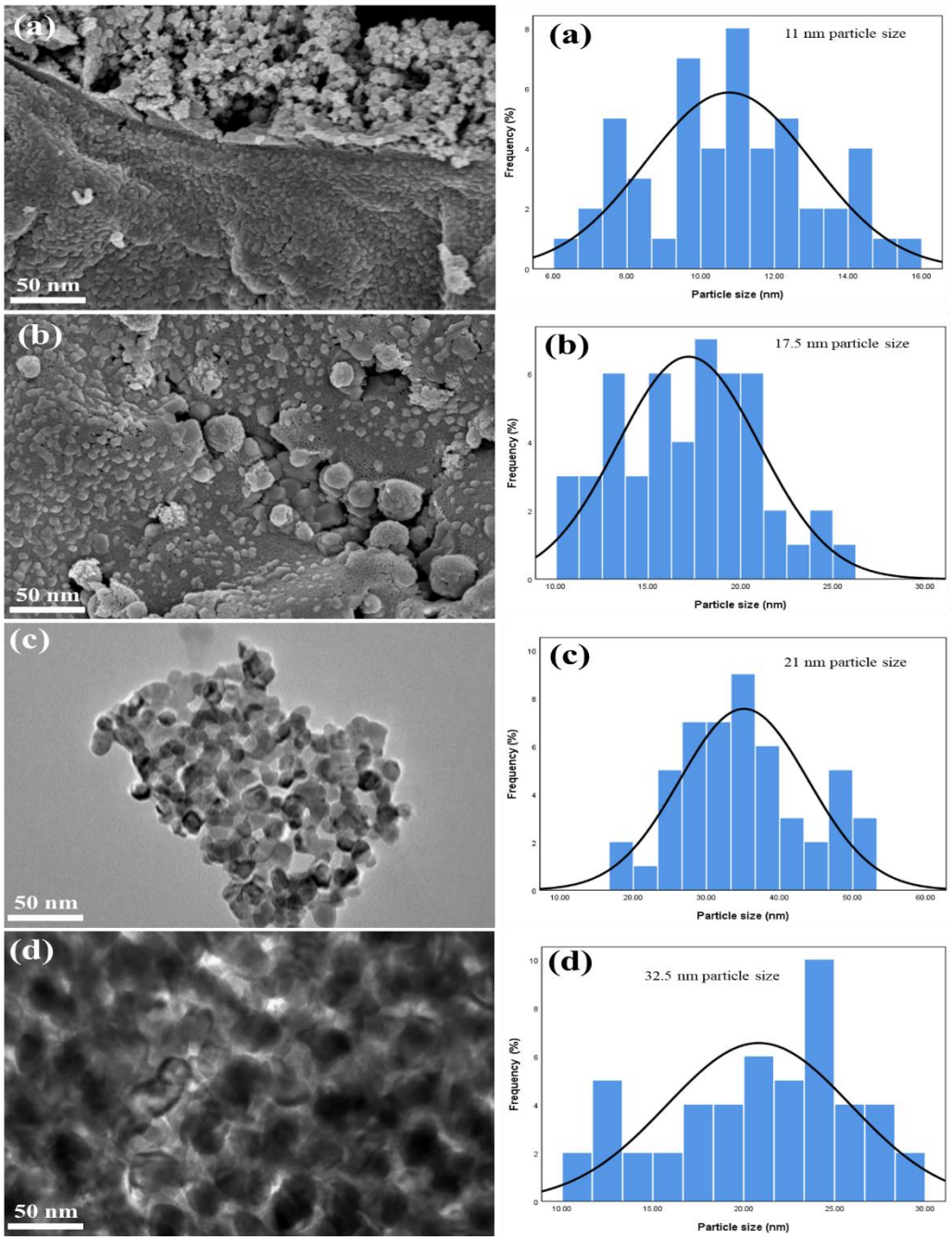

Figure 4: TEM analysis of $(ZnO)_{0.8}$ $(ZrO_2)_{0.2}$ nanocomposites and particle size distribution at varying calcination temperatures of (a) 500 ºC (b) 600 ºC (c) 700 ºC and (d) 800 ºC

Figure 5 illustrates the increase in particle size as the calcination temperature rises. The increase in particle size was caused by many nearby particles sticking together as a result of surface melting at a higher temperature (Alzahrani *et al.*, 2022). The crystallinity has grown as a result of the increase in nuclei's particle size caused by the increase in crystalline volume ratio. This allows one to draw the conclusion that the increase in

calcination temperature has caused the particle size volume to grow from 11.0 to 32.5 nm. As the calcination temperature rises, the estimation of crystallite increases allometrically (Keiteb *et al.*, 2016). The increase in molecule estimations is likely caused by a few neighbouring particles holding rapidly together owing to surface softening at higher temperatures (Kamari *et al.*, 2017). The estimated values fall within the range of nanocomposites in size.

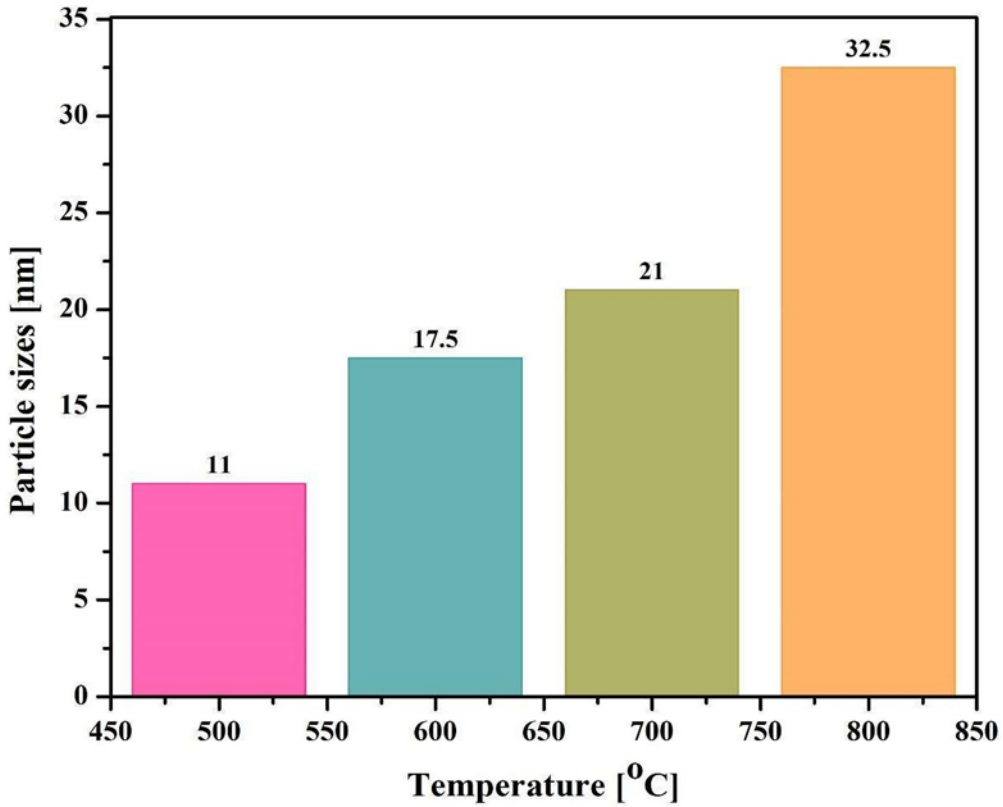

Figure 5: Calcination temperature and particle size (TEM) of $(ZnO)_{0.8}$ $(ZrO_2)_{0.2}$

Optical properties

Photoluminescence (PL)

Figure 6 shows the PL spectra of $(ZnO)_{0.8}(ZrO_2)_{0.2}$ nanocomposites calcined at 500°C, 600°C, 700°C, and 800°C exhibiting significant variations in optical emissions, reflecting the impact of calcination temperature on the material's crystallinity, defect states, and electronic structure. The observed emission peaks span from the ultraviolet (UV) to the visible region, indicating the presence of both near-band-edge (NBE) and deep-level emissions (DLE). The NBE emission, typically appearing around 380-400 nm, is attributed to excitonic recombination in ZnO Bandopadhyay and Mitra (2015), and tends to intensify with increasing calcination temperature. This enhancement suggests improved crystallinity due to higher temperature-induced grain growth, leading to a reduction in structural imperfections and non-radiative recombination pathways.

At lower calcination temperatures, such as 500°C and 600°C, the PL intensity is relatively weaker, which is likely due to the presence of residual organic impurities, lattice distortions, and a higher concentration of defects such as oxygen vacancies and zinc interstitials (Koebel *et al.*, 2008). These structural imperfections introduce deep-level states that facilitate non-radiative recombination, thereby reducing PL intensity. As the calcination temperature increases to 700°C and 800°C, the material undergoes significant structural reordering, resulting in larger, well-formed crystalline grains with fewer defects. This leads to a more intense NBE emission, indicative of enhanced optical quality.

The broad emission in the visible region (420-480 nm) corresponds to deep-level emissions (DLE), primarily originating from intrinsic defects such as oxygen vacancies, zinc interstitials, and zinc vacancies. The intensity of these deep-level emissions varies with calcination temperature, reflecting changes in the defect concentration. At moderate temperatures (600°C and 700°C), defect-related emissions remain prominent, suggesting that while crystallinity improves, some residual defect states persist. However, at 800°C, the intensity of the visible emissions slightly decreases, indicating a reduction in defect density due to enhanced

thermal diffusion and recombination of defect states, leading to an overall improvement in material quality.

The incorporation of ZrO_2 into the ZnO matrix plays a crucial role in modifying the PL response. ZrO_2, being a high-bandgap material, acts as a stabilizing agent, preventing excessive grain growth and providing defect passivation, which helps in maintaining a controlled defect environment. Additionally, the presence of ZrO_2 also influences the thermal stability of ZnO, allowing the composite material to retain its structural integrity at elevated temperatures (Chitoria *et al.*, 2023). The observed shifts in PL intensity and peak positions suggest that ZrO_2 incorporation alters charge carrier dynamics, potentially reducing defect-mediated recombination while enhancing excitonic transitions.

The PL analysis indicates that calcination at 700°C or 800°C provides an optimal balance between crystallinity and defect passivation, leading to enhanced optical properties. The reduced deep-level emissions at higher temperatures suggest improved structural quality, making these nanocomposites more suitable for optoelectronic and photocatalytic applications where high charge carrier mobility and minimal defect-mediated recombination are essential.

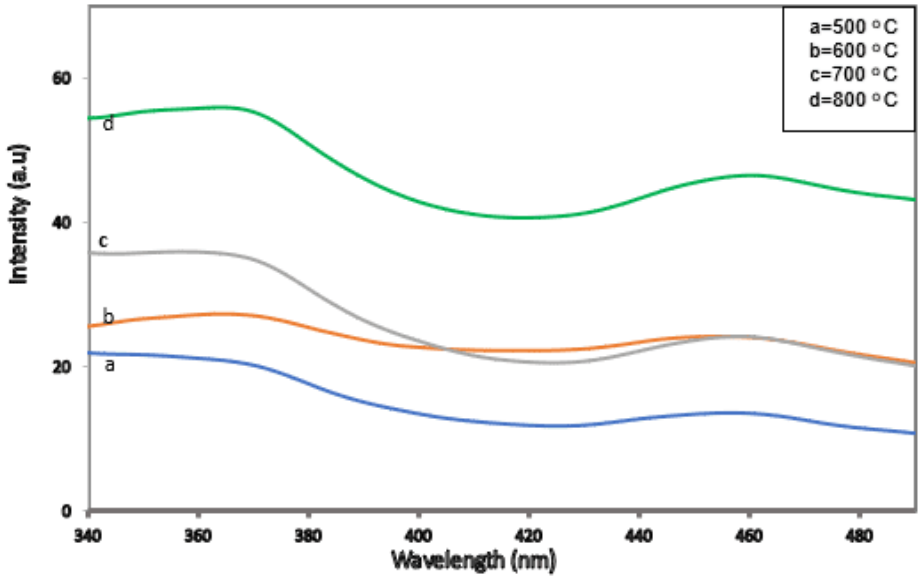

Figure 6: PL of $(ZnO)_{0.8}$ $(ZrO_2)_{0.2}$ calcinated at (a) 500 (b) 600 (c) 700 (d) 800 °C

CONCLUSION

In this study, ZnO-ZrO_2 nanocomposites were successfully synthesized using a controlled calcination method, and their structural and optical properties were systematically investigated. XRD analysis confirmed the coexistence of ZnO and ZrO_2 crystalline phases, with increased crystallinity observed at higher calcination temperatures. TEM imaging revealed uniform nanostructures, while PL spectroscopy indicated reduced electron-hole recombination, suggesting enhanced photocatalytic efficiency. These findings demonstrate that optimizing the ZnO:ZrO_2 ratio and calcination conditions can significantly improve the material's optoelectronic properties. The enhanced performance of ZnO-ZrO_2 nanocomposites highlights their potential for energy-efficient photocatalysis and other advanced applications in optoelectronics and environmental remediation. Future work should explore further optimization of synthesis parameters and assess the photocatalytic activity under real-world conditions to validate their practical applicability.

ACKNOWLEDGEMENT

We acknowledged department of Physics, University Putra Malaysia for the opportunity given to us to carry out this research work.

REFERENCES

Al-Hada, N. M., Saion, E., Kamari, H. M., Flaifel, M. H., Shaari, A. H., Talib, Z. A., Abdullahi, N., Baqer, A. A., & Kharazmi, A. (2016). Structural, morphological and optical behaviour of PVP capped binary (ZnO) 0.4 (CdO) 0.6 nanoparticles synthesised by a facile thermal route. *Materials Science in Semiconductor Processing*, *53*, 56-65. https://doi.org/10.1016/j.mssp.2016.06.004

Al-Hada, N. M., Saion, E. B., Shaari, A. H., Kamarudin, M. A., Flaifel, M. H., Ahmad, S. H., & Gene, S. A. (2014). A facile thermal-treatment route to synthesize ZnO nanosheets and effect of calcination temperature. *PloS one*, *9*(8), e103134. https://doi.org/10.1371/journal.pone.0103134

Alzahrani, J. S., Midala, I. H., Kamari, H. M., Al-Hada, N. M., Tim, C. K., Nidzam, N. N. S., Alrowaili, Z., & Al-Buriahi, M. (2022). Effect of Calcination Temperature on the Structural and Optical Properties of (ZnO) 0.8 (ZrO2) 0.2 Nanoparticles. *Journal of Inorganic and Organometallic Polymers and Materials*, *32*(5), 1755-1765. https://doi.org/10.1007/s10904-022-02238-8

Bandopadhyay, K., & Mitra, J. (2015). Zn interstitials and O vacancies responsible for n-type ZnO: what do the emission spectra reveal? *Rsc Advances*, *5*(30), 23540-23547. https://doi.org/10.1039/C5RA00355E

Cairns, A. B., & Goodwin, A. L. (2013). Structural disorder in molecular framework materials. *Chemical society reviews*, *42*(12), 4881-4893. https://doi.org/10.1039/C3CS35524A

Chitoria, A. K., Mir, A., & Shah, M. (2023). A review of ZrO2 nanoparticles applications and recent advancements. *Ceramics international*. https://doi.org/10.1016/j.ceramint.2023.06.296

Deepika, R., & Veerakumar, P. (2024). Microwave-assisted hydrothermal synthesis of ZnO@ ZrO2 nanohybrid for biomedical and photocatalytic applications. *Colloids and Surfaces A: Physicochemical and Engineering Aspects*, *688*, 133574. https://doi.org/10.1016/j.colsurfa.2024.133574

Gene, S. A., Saion, E. B., Shaari, A. H., Kamarudeen, M. A., & Al-Hada, N. M. (2015). RETRACTED: Fabrication and Characterization of Nanospinel ZnCr2O4 Using Thermal Treatement Method. *Advanced materials research*, *1107*, 301-307. https://doi.org/10.1155/2014/416765

Goodarz Naseri, M., Saion, E. B., & Kamali, A. (2012). An overview on nanocrystalline ZnFe2O4, MnFe2O4, and CoFe2O4 synthesized by a thermal treatment method. *International Scholarly Research Notices*, *2012*. https://doi.org/10.5402/2012/604241

Gurushantha, K., Renuka, L., Anantharaju, K., Vidya, Y., Nagaswarupa, H., Prashantha, S., & Nagabhushana, H. (2017). Photocatalytic and photoluminescence studies of ZrO2/ZnO nanocomposite for LED and waste water treatment applications. *Materials Today: Proceedings*, *4*(11), 11747-11755. https://doi.org/10.1016/j.matpr.2017.09.091

Kamari, H. M., Al-Hada, N. M., Baqer, A. A., Shaari, A. H., & Saion, E. (2019). Comprehensive study on morphological, structural and optical properties of Cr 2 O 3 nanoparticle and its antibacterial activities. *Journal of Materials Science: Materials in Electronics*, *30*, 8035-8046. https://doi.org/10.1007/s10854-019-01125-2

Kamari, H. M., Al-Hada, N. M., Saion, E., Shaari, A. H., Talib, Z. A., Flaifel, M. H., & Ahmed, A. A. A. (2017). Calcined solution-based PVP influence on ZnO semiconductor nanoparticle properties. *Crystals*, *7*(2), 2. https://doi.org/10.3390/cryst7020002

Kayani, Z. N., Saleemi, F., & Batool, I. (2015). Effect of calcination temperature on the properties of ZnO nanoparticles. *Applied Physics A*, *119*, 713-720. https://doi.org/10.1007/s00339-015-9019-1

Keiteb, A. S., Saion, E., Zakaria, A., & Soltani, N. (2016). Structural and optical properties of zirconia nanoparticles by thermal treatment synthesis. *Journal of Nanomaterials*, *2016*(1), 1913609. https://doi.org/10.1155/2016/1913609

Kocjan, A., Logar, M., & Shen, Z. (2017). The agglomeration, coalescence and sliding of nanoparticles, leading to the rapid sintering of zirconia nanoceramics. *Scientific reports*, *7*(1), 2541. https://doi.org/10.1038/s41598-017-02760-7

Koebel, M. M., Jones, L. C., & Somorjai, G. A. (2008). Preparation of size-tunable, highly monodisperse PVP-protected Pt-nanoparticles by seed-mediated growth. *Journal of Nanoparticle Research*, *10*(6), 1063-1069. https://doi.org/10.1007/s11051-008-9370-7

Kubiak, A., Siwińska-Ciesielczyk, K., & Jesionowski, T. (2018). Titania-based hybrid materials with ZnO, ZrO2 and MoS2: A review. *Materials*, *11*(11), 2295. https://doi.org/10.3390/ma11112295

Lee, K. M., Lai, C. W., Ngai, K. S., & Juan, J. C. (2016). Recent developments of zinc oxide based photocatalyst in water treatment technology: a review. *Water research*, *88*, 428-448. https://doi.org/10.1016/j.watres.2015.09.045

Liao, M.-H., Hsu, C.-H., & Chen, D.-H. (2006). Preparation and properties of amorphous titania-coated zinc oxide nanoparticles. *Journal of Solid State Chemistry*, *179*(7), 2020-2026. https://doi.org/10.1016/j.jssc.2006.03.042

López, U., Lemus, A., Hidalgo, M., López González, R., Quintana Owen, P., Oros-Ruiz, S., Uribe López, S., & Acosta, J. (2019). Synthesis and characterization of ZnO-ZrO2 nanocomposites for photocatalytic degradation and mineralization of phenol. *Journal of Nanomaterials*, *2019*. https://doi.org/10.1155/2019/1015876

Maaz, K., Karim, S., Mumtaz, A., Hasanain, S., Liu, J., & Duan, J. (2009). Synthesis and magnetic characterization of nickel ferrite nanoparticles prepared by co-precipitation route. *Journal of Magnetism and Magnetic Materials*, *321*(12), 1838-1842. https://doi.org/10.1016/j.jmmm.2008.11.098

Mariyappillai, V., Shiyamala, C., Abisheik, T., Tiffany, M., Pandiyan, V., Senthilraja, A., Afzal, M., Barmavatu, P., Shanmugaraj, K., & Balu, K. (2025). Zr-modified ZnO nanoparticles: Optimized photocatalytic degradation and antibacterial efficiency for pollution control. *Ceramics international*. https://doi.org/10.1016/j.ceramint.2025.02.402

Midala, I. H., Kamari, H. M., Al-Hada, N. M., Tim, C. K., Muhamad, S., Hamza, A. M., Abubakar, T. R., & Nuhu, I. M. (2019). Structural, morphological and optical properties of (ZnO) 0.2 (ZrO2) 0.8 nanoparticles. *Applied Physics A*, *125*(9), 1-10. https://doi.org/10.1007/s00339-019-2950-9

Park, S., Kim, C.-H., Lee, W.-J., Sung, S., & Yoon, M.-H. (2017). Sol-gel metal oxide dielectrics for all-solution-processed electronics. *Materials Science and Engineering: R: Reports*, *114*, 1-22. https://doi.org/10.1016/j.mser.2017.01.003

Precious Ayanwale, A., & Reyes-López, S. n. Y. (2019). ZrO2–ZnO nanoparticles as antibacterial agents. *ACS omega*, *4*(21), 19216-19224. http://dx.doi.org/10.1021/acsomega.9b02527

Sathyaseelan, B., Manikandan, E., Baskaran, I., Senthilnathan, K., Sivakumar, K., Moodley, M., Ladchumananandasivam, R., & Maaza, M. (2017). Studies on structural and optical properties of ZrO2 nanopowder for opto-electronic applications. *Journal of alloys and compounds*, *694*, 556-559. https://doi.org/10.1016/j.jallcom.2016.10.002

Shakir, H. A., Alsaffar, M. A., Mageed, A. K., Sukkar, K. A., & Ghany, M. A. A. (2024). Optimizing Photocatalytic Lead Removal from Wastewater Using ZnO/ZrO2: A Response Surface Methodology Approach. *ChemEngineering*, *8*(4), 72. https://doi.org/10.3390/chemengineering8040072

Sherly, E., Vijaya, J. J., Selvam, N. C. S., & Kennedy, L. J. (2014). Microwave assisted combustion synthesis of coupled ZnO–ZrO2 nanoparticles and their role in the photocatalytic degradation of 2, 4-dichlorophenol. *Ceramics international*, *40*(4), 5681-5691. https://doi.org/10.1016/j.ceramint.2013.11.006.

Sun, Y., Zhang, W., Li, Q., Liu, H., & Wang, X. (2023). Preparations and applications of zinc oxide based photocatalytic materials. *Advanced Sensor and Energy Materials*, 100069. https://doi.org/10.1016/j.mseb.2021.115363

Terna, A. D., Elemike, E. E., Mbonu, J. I., Osafile, O. E., & Ezeani, R. O. (2021). The future of semiconductors nanoparticles: Synthesis, properties and applications. *Materials Science and Engineering: B*, *272*, 115363. https://doi.org/10.1016/j.mseb.2021.115363

Ullah, A., Ahn, C. W., Hussain, A., & Kim, I. W. (2010). The effects of sintering temperatures on dielectric, ferroelectric and electric field-induced strain of lead-free Bi0. 5 (Na0. 78K0. 22) 0.5 TiO3 piezoelectric ceramics synthesized by the sol–gel technique. *Current Applied Physics*, *10*(6), 1367-1371. https://doi.org/10.1016/j.cap.2010.05.004

Vickers, M., Kappers, M., Datta, R., McAleese, C., Smeeton, T., Rayment, F., & Humphreys, C. (2005). In-plane imperfections in GaN studied by x-ray diffraction. *Journal of Physics D: Applied Physics*, *38*(10A), A99. https://doi.org/10.1088/0022-3727/38/10A/019

Vitor, G., Palma, T., Vieira, B., Lourenço, J., Barros, R., & Costa, M. C. (2015). Start-up, adjustment and long-term performance of a two-stage bioremediation process, treating real acid mine drainage, coupled with biosynthesis of ZnS nanoparticles and ZnS/TiO2 nanocomposites. *Minerals Engineering*, *75*, 85-93. https://doi.org/10.1016/j.mineng.2014.12.003

Wante, H. P., Aidan, J., & Ezike, S. C. (2021). Efficient dye-sensitized solar cells (DSSCs) through atmospheric pressure plasma treatment of photoanode surface. *Current Research in Green and Sustainable Chemistry*, *4*, 100218. https://doi.org/10.1016/j.crgsc.2021.100218

Yousefi, R., Beheshtian, J., Seyed-Talebi, S. M., Azimi, H., & Jamali-Sheini, F. (2018). Experimental and theoretical study of enhanced photocatalytic activity of Mg-doped ZnO NPs and ZnO/rGO nanocomposites. *Chemistry–An Asian Journal*, *13*(2), 194-203. https://doi.org/10.1002/asia.201701423

Zhang, Q., Xu, X., Liu, Y., Xu, M., Deng, S., Chen, Y., Yuan, H., Yu, F., Huang, Y., & Zhao, K. (2017). A feasible strategy to balance the crystallinity and specific surface area of metal oxide nanocrystals. *Scientific reports*, *7*(1), 46424. https://doi.org/10.1038/srep46424.